ELECTRONIC SUPPLEMENTARY INFORMATION

for:

Self-diffusion in Isotropic and Liquid Crystalline Phases of fd Virus Colloidal Rods: a Combined Single Particle Tracking and Differential Dynamic Microscopy Study

Details for extracting long time diffusion coefficients with DDM

As briefly outlined in the main text, anisotropic DDM analysis was performed on well aligned sub-regions selected through visual inspection. The direction of slowest dynamics is easily identified as a 'low signal line' in the 2D DICF at short delay times (Fig. S1A). This corresponds to the direction perpendicular to the rod axis, and was experimentally found to be consistent with the visually identified rod direction in the fluorescence movies (*i.e.* perpendicular to it). We then used 12 angular sectors of $\Delta\theta = 15°$ width centred on this direction for further analysis. Averaging these sets of $g(q,\theta,\tau)$ for several ROIs helped to increase the signal-to-noise ratio.

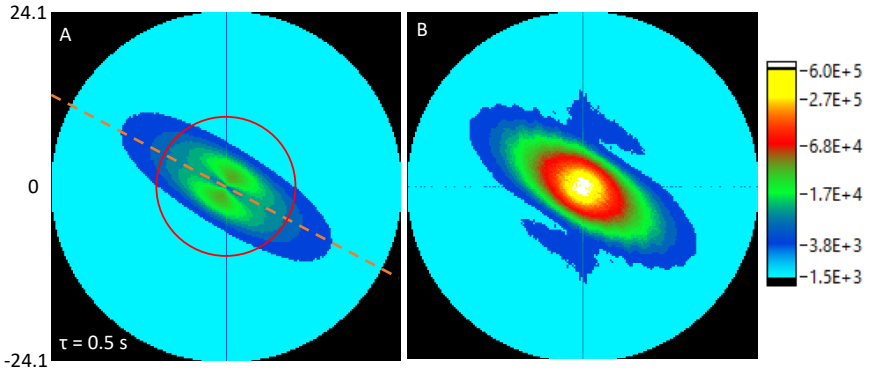

Fig. S1 DICF spectra for a densely labelled sample in the smectic phase. (A) After a short delay time the direction of slow dynamics can be easily identified (dashed orange line). (B) After a very long delay, where the signal amplitude can be used to estimate the square of the virus' form factor. The q range of both spectra is $\pm 24.1\,\mu\mathrm{m}^{-1}$ and the DDM signal amplitude is visualised using a logarithmic colour scale as indicated. Note that for the green labelled samples we could only analyse a much smaller q range as indicated by the red circle.

Representative DICF's are shown in Fig. S2 for both isotropic and nematic samples.

In the low q-limit, the long time diffusion coefficient $D(\theta)$ was estimated by fitting

$$\Gamma(q,\theta) = \Gamma_0(\theta) + D(\theta)q^2, \tag{S1}$$

over a suitable range of q values (Fig. S3).

For isotropic samples there was no need for sector based analysis, and the decay constant initially scales linearly with q^2, as expected for purely diffusive dynamics. But as can be seen from Fig. S3A, with increasing density there is clear deviation from this initially linear trend for large q^2. Here we used a linear fit up to $q^2 = 4\mu\mathrm{m}^{-2}$ to estimate the long time diffusion coefficient.

For nematic samples the decay rates vary with θ, *i.e.* the direction of motion within the observation plane. Fig. S3B shows some representative data for motion in the parallel and perpendicular direction for three different concentrations. The slow dynamics in the perpendicular direction shows diffusive scaling over the complete q^2 range, whereas the decay rates in the parallel direction can only be extracted up to about $10\,\mu\mathrm{m}^{-2}$. This shorter range is due to a drop in signal levels caused by the more pronounced effect of the form factor while the decay rate approaches the frame rate of the movie (33 fps). In the smectic phase (Fig. S3C) the overall dynamics is even slower and the scaling in the parallel direction fails at much lower q^2 values. The small offset Γ_0 becomes clearly noticeable here.

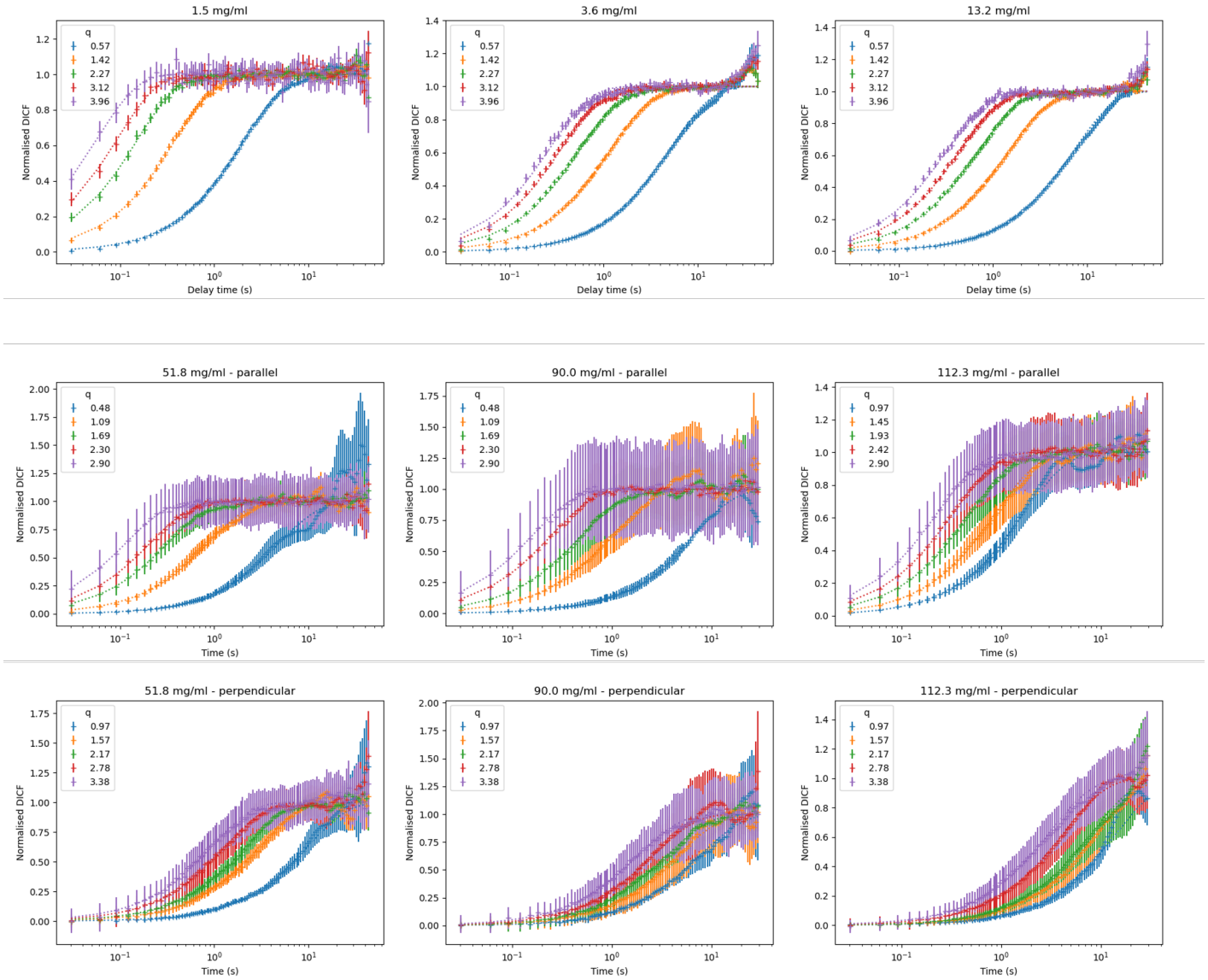

Fig. S2 Normalised DICFs for different sample concentrations for a range of q-values (symbols) together with fit curves assuming a diffusive ISF (dotted lines). The top row shows DICFs for three isotropic samples: as the data can be averaged over all azimuthal angles the experimental data has relatively small error bars. For nematic samples the DICF becomes direction dependent: The second row shows the (faster) dynamics parallel to the director and the third row the corresponding data in the perpendicular direction. Note that the data are noisier due to the poorer statistics afforded by averaging over 15° angular sectors.

For both the nematic and smectic phases we extracted the long time diffusion coefficient in the parallel direction by fitting Eq. S1 up to $q^2 = 4\mu\text{m}^{-2}$ and used the whole range for the perpendicular direction.

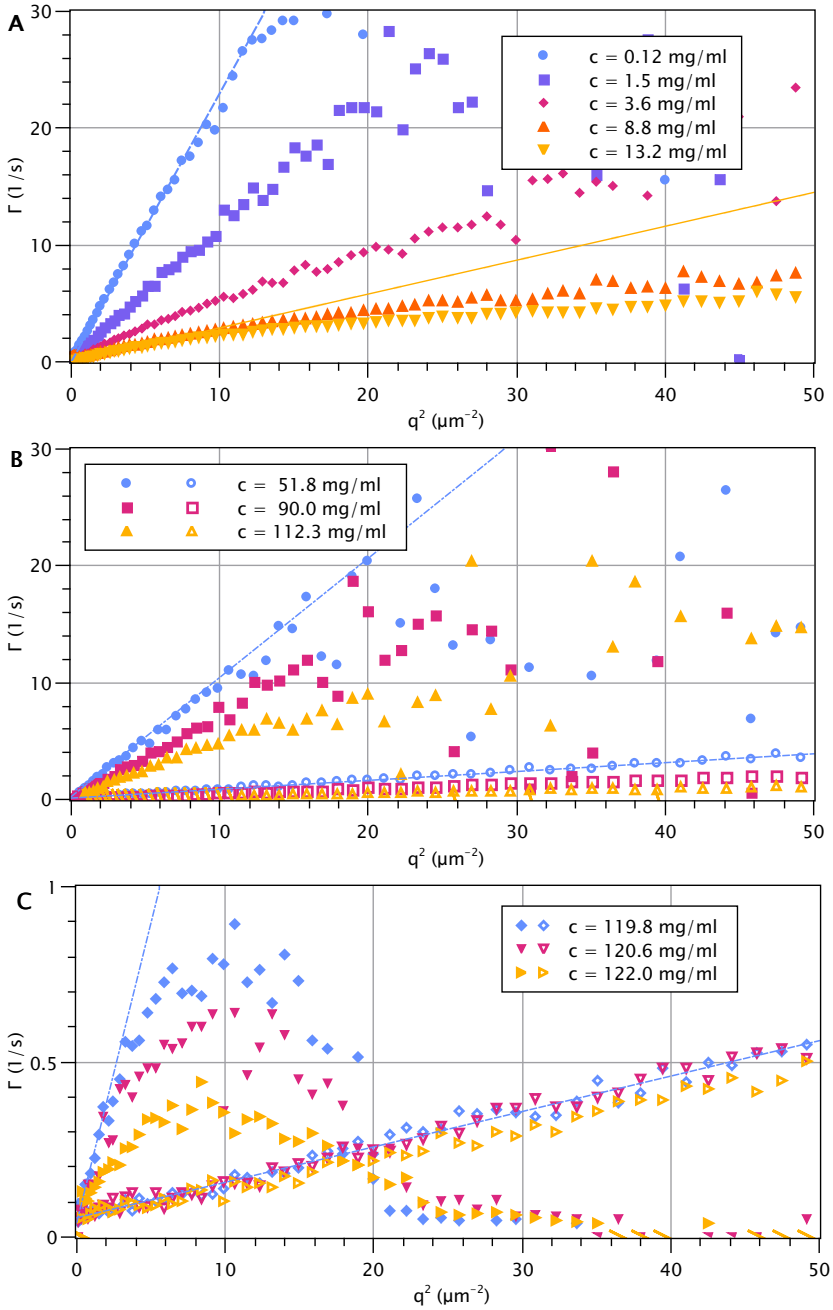

Fig. S3 Decay constants Γ plotted against q^2 for several sample concentrations within the (A) isotropic, (B) nematic and (C) smectic phase. In panels (B) & (C) the filled symbols are for motion parallel to the virus long axis and the open symbols for the much slower motion in the perpendicular direction.

DICFs for red labelled smectic sample

The improved contrast and increased density of labelled viruses allows us to extract much cleaner DICFs, as shown in Fig. S4. In the perpendicular direction smectic samples retain simple exponential ISFs for all q and the DICFs collapse when plotted against delay time scaled by q^2, confirming that its dynamics is purely diffusive. But in the parallel direction we can now clearly see deviations a simple exponential ISF. A stretched exponential fit captures the dominant dynamics well (Fig. S4 B&E), however for $q \gtrsim 4\mu\text{m}^{-1}$, close to length scale $1/q$ associated with the layer spacing, two distinct decay processes can be visually identified. Using a double-exponential fit,

$$f(q,\tau) = (1-\alpha)\, e^{-D_{\text{fast}} q^2 \tau} + \alpha\, e^{-D_{\text{fast}} q^2 \tau}\,, \tag{S2}$$

both processes are captured well for $4\mu\text{m}^{-1} < q < 5.1\mu\text{m}^{-1}$, where the faster process has $D_{\text{fast}} \approx 0.26(5)\mu\text{m}^2/\text{s}$ and the dominant slower process $D_{\text{slow}} \approx 0.014(6)\mu\text{m}^2/\text{s}$, with a fractional contribution $\alpha \approx 0.65$ to the overall signal (Fig. S5). Note that there is no *a priori* reason to assume that these processes are diffusive. However, to extract physical insights from the use of a double-stretched fit model (*i.e.* a superposition of two stretched exponentials) a more systematic study would be needed, as well as access to shorter delay times.

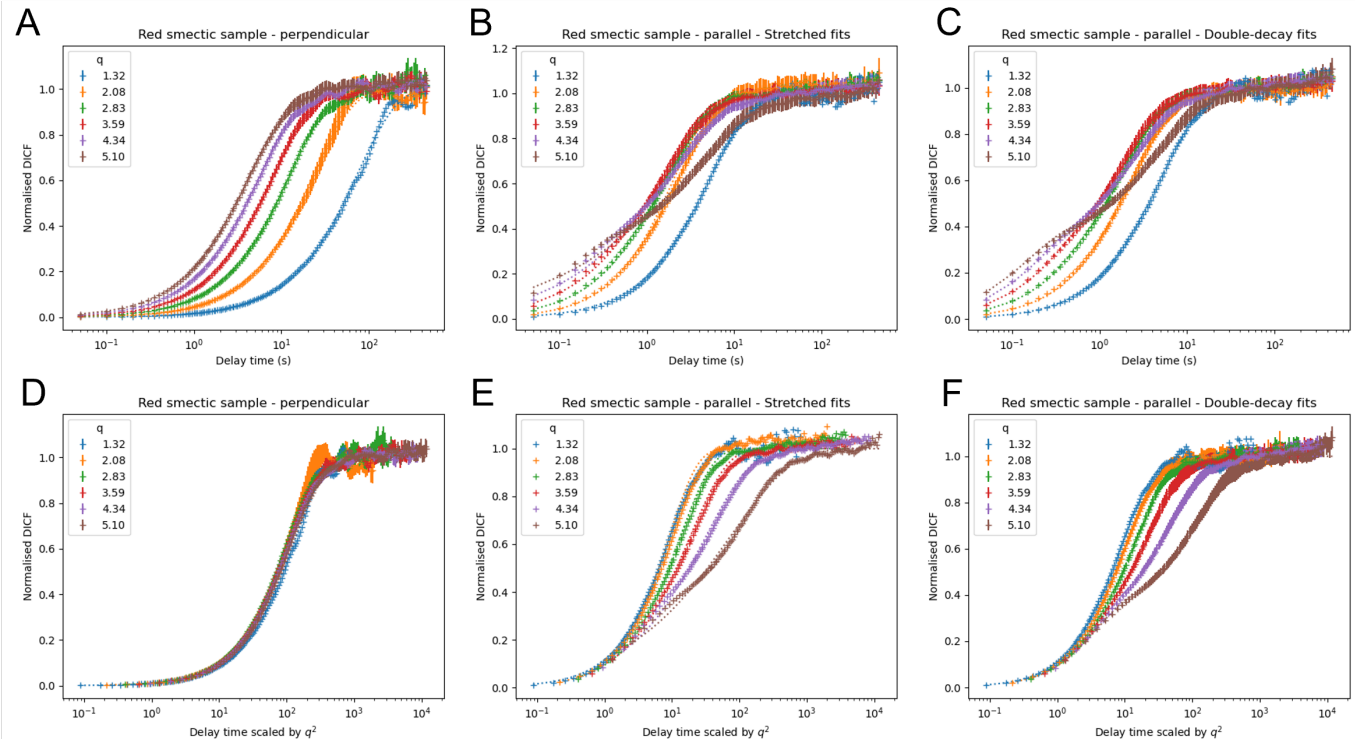

Fig. S4 Normalised DICFs for selected q values for the densely red labelled sample in the smectic phase. Corresponding fit curves are displayed as dotted lines. Top left plot (A) shows DICFs for motion perpendicular to the director. The middle (B) and right (C) plots are for motion parallel to the director together with a stretched fit or double-exponential fit, respectively. The bottom row (D-F) shows the same data but with the delay time scaled by q^2. Note that panel (E) does not show error bars to make systematic deviations of stretched fit more visible.

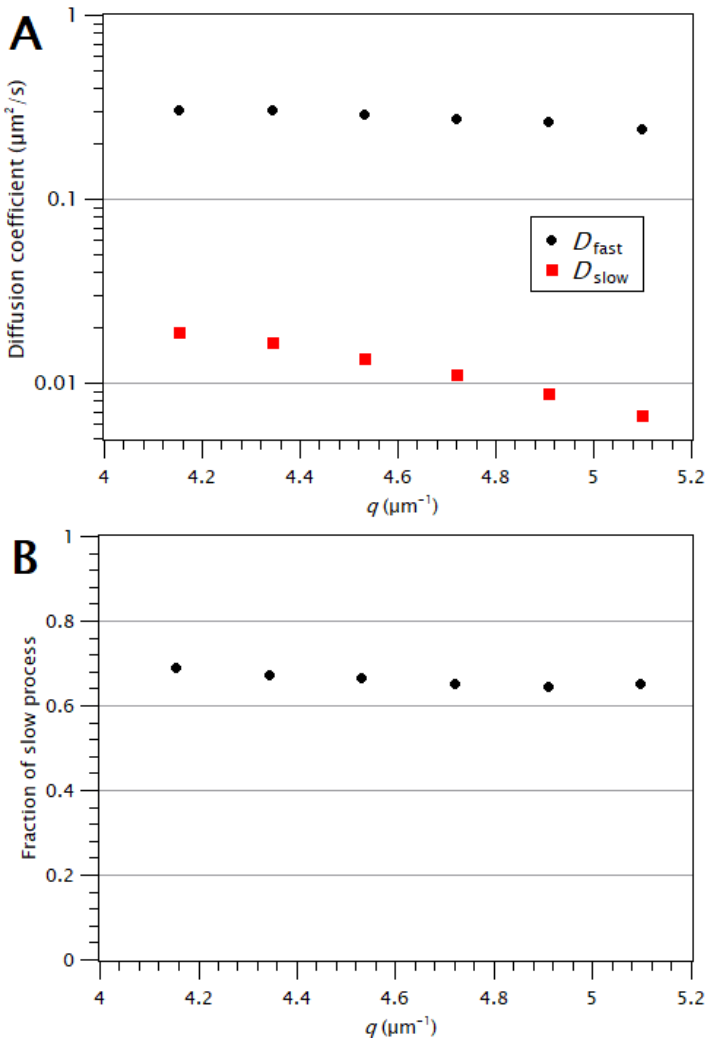

Fig. S5 (A) Diffusion coefficients and (B) fractional contribution of the slow process (α, see Eq. S2) for a double-exponential fit to the DICF in the parallel direction.

Details for extracting long time diffusion coefficients from MSD by SPT

The mean squared displacements (MSD) averaged over hundreds of traces obtained by SPT (see main text), are fitted to determine the corresponding anisotropic diffusion coefficients $D_{\parallel}$ and $D_{\perp}$ in the direction parallel $\parallel$ and perpendicular $\perp$ to the mean rod orientation, respectively.[23] As numerical fit, a power law is used with a constant offset, assumed to be isotropic, and accounting for the finite optical (point spread function) and temporal resolution of the optical setup. As displayed in Fig. S6, most the dynamics of the system is diffusive for the probed time window in the nematic phase for both directions, and in the smectic phase for the perpendicular direction. However, for the smectic phase in the parallel direction, a sub-diffusive regime can be evidenced at short time associated with the hopping-type motion, whereas a diffusive regime is recovered at long time (Red full circle symbols in Fig. S6).

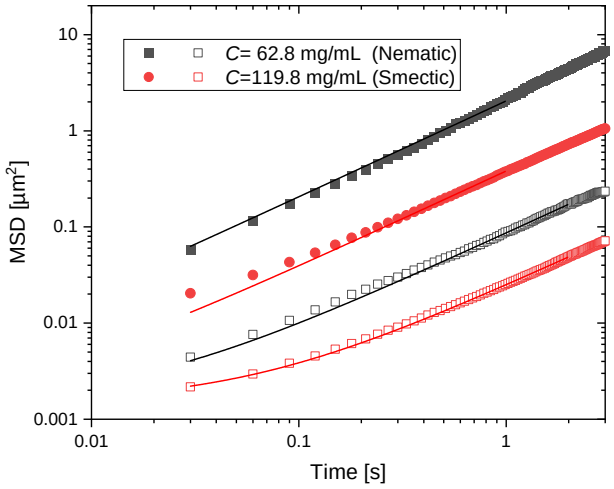

Fig. S6 Mean squared displacements as a function of time for two virus concentrations of $C = 62.8$ mg/mL and $C = 119.8$ mg/mL corresponding to the nematic (black symbols) and smectic (red symbols) liquid crystalline phases, respectively. The filled symbols are for parallel displacements along the virus director and the open symbols are for the perpendicular displacements. The continuous lines are diffusive fits with a fixed offset for both concentrations and directions: $MSD_{\parallel,\perp} = 2D_{\parallel,\perp}t + 0.0015\,\mu m^2$. The small offset accounts for the dynamic localisation uncertainty.

Estimating the form factor from the DDM signal amplitude

At large delay times τ the amplitude of the DICF spectrum as shown in Fig. S1 B reveals the $\mathbf{q}$-variation of the signal amplitude $A(\mathbf{q})$. Fig. S7 shows the amplitudes for 12 sectors, with the magenta data points corresponding to motion along the virus axis, $A_{\parallel}(q)$ at $\theta = 0°$ and the black symbols to motion in the perpendicular direction, $A_{\perp}(q)$ (θ =90°). As the physical diameter of the virus is well below the resolution limit of the microscope, *i.e.* $P_{\perp}(q) = 1$ throughout the accessible q-range, the observed q dependence of $A_{\perp}$ is only due to the optical transfer function of the objective. By calculating the ratio

$$\frac{A_{\parallel}(q)}{A_{\perp}(q)} = \frac{N\kappa^2|\mathrm{OTF}(q)|^2\,|P_{\parallel}(q)|^2}{N\kappa^2|\mathrm{OTF}(q)|^2} = |P_{\parallel}(q)|^2$$

we can therefore get an estimate of the square of the form factor of the virus, as shown in Fig. 5 in the main manuscript.

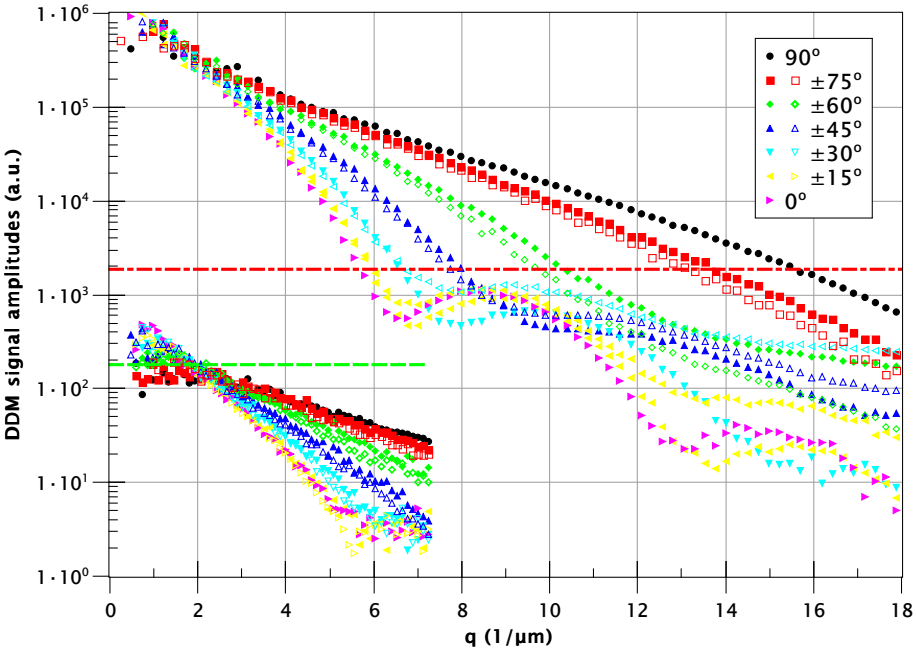

Fig. S7 DDM signal amplitudes as a function of direction relative to the virus director. The signal for motion perpendicular to the virus axis (black dots) drops much more slowly than in the parallel direction (magenta right triangles), for which pronounced minima can be distinguished due to the viruses form factor. The main dataset (with larger signal amplitude spanning a much wider q-range) is from a very long movie recorded with red labelled viruses in the smectic phase (see main text). A representative dataset for movies with viruses labelled with green fluorescent dyes, as used for the majority of experimental data presented here, is also shown for comparison. The horizontal dashed lines indicate the average value of background $B(q)$ (see Eq. 2) for the respective datasets.